ASCE

Estimating Impacts of Dam Development and Landscape Changes on Suspended Sediment Concentrations in the Mekong River Basin's 3S Tributaries

Claire Beveridge[1]; Faisal Hossain[2]; and Matthew Bonnema[3]

Abstract: The Mekong River Basin (MRB) is undergoing rapid dam development, which is altering the river suspended sediment concentration (SSC). In this study, we used satellite remote sensing records spanning 31 years to detect SSC changes (SSC prediction $r^2 = 0.78$, RMSE $= 21.2$ mg/L) due to dam development. We focused on the 3S basin of the MRB. We also used satellite data on nighttime lights, which reflect human settlement patterns, and land cover to explain SSC patterns. Our technique allowed for quantification of SSC changes due to dam construction (e.g., +120 mg/L near basin outlet), reservoir sediment trapping (e.g., −108 mg/L), deforestation, and human settlement (e.g., +117 mg/L near impacts). Our technique also demonstrated how the SSC of the 3S rivers compared to that of the Mekong mainstem over time (e.g., from ∼13% to 100% greater). Our comprehensive analyses of SSC records with dam development indicate that SSC changes will continue with ongoing dam and landscape development in the MRB. From a hydrologic perspective, SSC monitoring will be imperative for effective sediment and water management. Our satellite-based approach answers critical sediment needs of improved monitoring and adaptive management throughout the MRB and other global locations for practitioners who are engaged in real-world management of their river basins. **DOI:** **10.1061/(ASCE)HE.1943-5584.0001949.**

Author keywords: Suspended sediment concentrations; Landsat; Dam development; Mekong; 3S rivers.

Introduction

The Mekong River Basin (MRB), shown in Fig. 1, is a complex environmental and social system that spans six countries, hosts rich biodiversity, and has a population of approximately 70 million people. Suspended sediment is critical to the highly productive ecosystem, fisheries, and agriculture of the MRB. However, rapid dam development in the MRB is significantly altering suspended sediment transport. If all planned MRB dams are constructed and no reservoir sediment management measures are taken, it is estimated that dams will trap 96% of the basin's suspended sediment yield (Kondolf et al. 2014). Valuable nutrient loads of nitrogen and phosphate that are carried by suspended sediment are also estimated to decline by 47%–62% (Piman and Shrestha 2017). Thus, although dams provide numerous benefits such as hydropower and irrigation, they are a major threat to the MRB environment, regional food security, and the vast number of natural resource-based livelihoods. Furthermore, the trapping of sediment in reservoirs decreases the lifespan of dams and compromises the intended benefits.

Most MRB dam projects do not have practices in place to address upstream and downstream impacts of dams on sediment throughout the various dam lifecycle stages (Piman and Shrestha 2017). At these different times and locations, dam impacts can be highly variable (e.g., channel aggradation or degradation) depending on river properties, sediment properties, dam construction and operation approaches, and compounding effects of dam sequences (Brandt 2000; Xu and Yan 2010; Lu et al. 2015; Kong et al. 2017). Considering the complexity of dam impacts, there is an urgent need for strategies to sustainably monitor and manage suspended sediment throughout the MRB. The existing in situ suspended sediment monitoring system of the MRB is limited in its spatial and temporal coverage as well as its reliability (e.g., Walling 2008). As a result, there is poor understanding of the baseline sediment conditions and the incremental impacts of dams and other landscape changes (Piman and Shrestha 2017). The development of effective suspended sediment management and mitigation measures is thereby limited. The monitoring, evaluation, and management strategies that are needed must be relevant to the spatial and temporal scales at which water, land, and dam management practices are implemented, and must be sustainable for the long term (Kong et al. 2017). Strategies must also be conducive to broader coordination between agencies, from the local to international levels (MRC 2017). Furthermore, as the environment, society, and technology continue to evolve, monitoring and management strategies must be adaptable.

Satellite remote sensing offers a practical response to sustainable sediment monitoring and management needs in the MRB. Satellite remote sensing offers extensive spatial coverage, frequent and extensive temporal records, cost effectiveness, and readily transferable data and methods. Satellite remote sensing has been broadly applied, as reported in the literature, for monitoring suspended sediment concentrations (SSC) of water bodies due to the relationship between SSC and satellite remote sensing visible and near-infrared (NIR) bands (e.g., Ritchie et al. 1987; Pavelsky and Smith 2009; Zhang et al. 2014; Gholizadeh et al. 2016; Yepez et al. 2018). Within the MRB, satellite remote sensing has also been used to quantify SSC in river channels (Suif et al. 2016; Markert et al. 2018) and in the Mekong Delta (Wackerman et al. 2017;

[1]Dept. of Civil and Environmental Engineering, Univ. of Washington, More Hall 201, Box 352700, Seattle, WA 98195. ORCID: https://orcid.org/0000-0002-6257-040X

[2]Dept. of Civil and Environmental Engineering, Univ. of Washington, More Hall 201, Box 352700, Seattle, WA 98195 (corresponding author). ORCID: https://orcid.org/0000-0001-6192-3157. Email: fhossain@uw.edu

[3]NASA Jet Propulsion Laboratory, Pasadena, CA.

Note. This manuscript was submitted on November 14, 2019; approved on February 14, 2020No Epub Date. Discussion period open until 0, 0; separate discussions must be submitted for individual papers. This paper is part of the *Journal of Hydrologic Engineering*, © ASCE, ISSN 1084-0699.

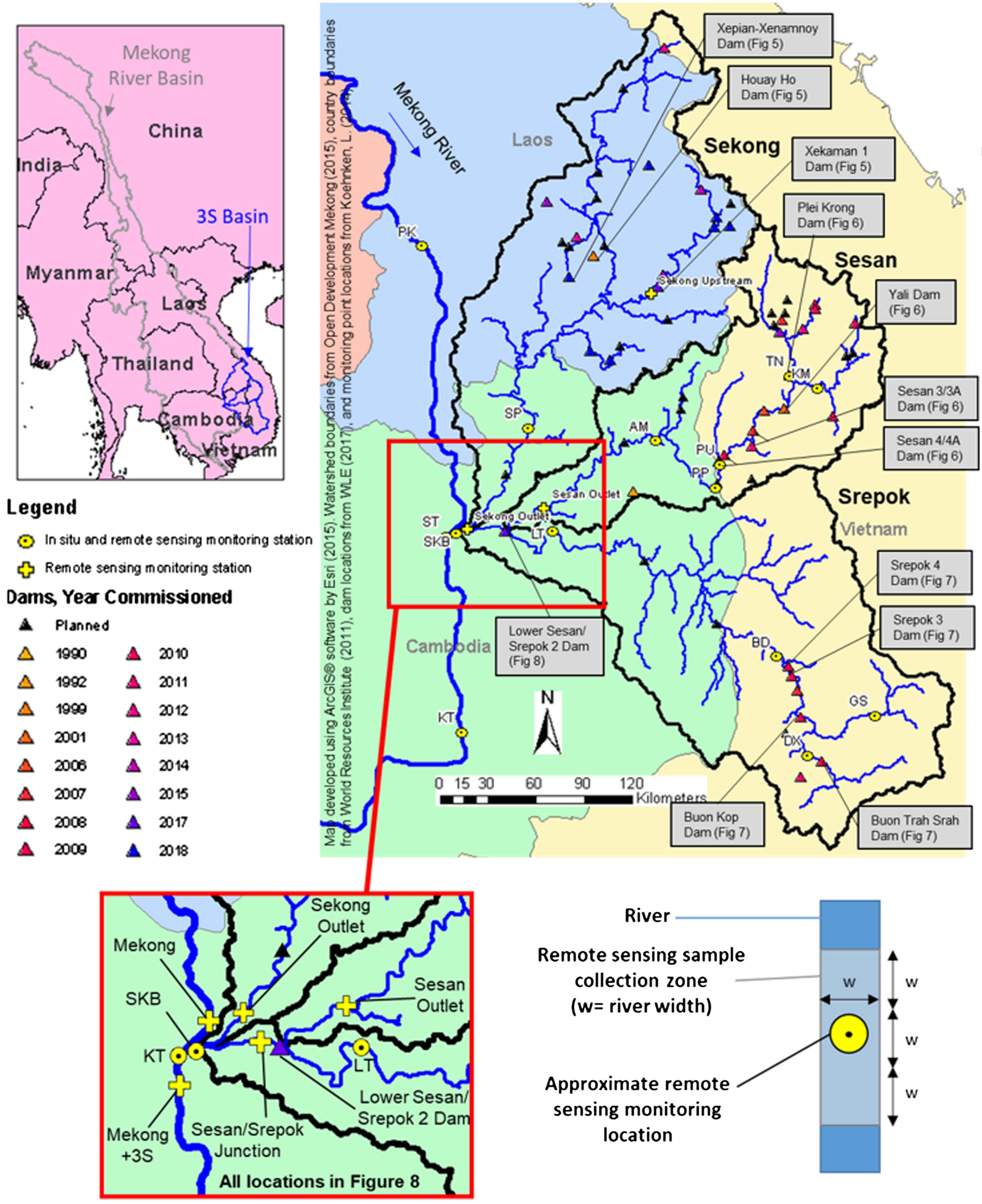

Fig. 1. Sekong, Sesan, and Srepok (3S) tributaries of the Mekong River Basin with dams and monitoring points. [Maps developed using ArcGIS software (Esri, Redlands, California). Watershed boundaries from Open Development Mekong (2015). Country boundaries from World Resources Institute (2011). Dam locations from WLE (2017). Monitoring point locations from Koehnken (2014).]

Dang et al. 2018). Collectively, these applications and advances in using satellite remote sensing for estimating SSC provide a platform for responding to practical engineering and management needs.

In this study, satellite remote sensing was used to detect SSC changes due to dam and landscape development in a subbasin of the MRB. The focus was the Sekong, Sesan, and Srepok tributaries, collectively known as the 3S basin (Fig. 1). The 3S basin is a valuable case study area because it provides the largest tributary contribution of sediment and streamflow to the Lower MRB (Kondolf et al. 2011), and thus has a vital role in the broader MRB ecosystem. The 3S basin is also a microcosm for dam development in the MRB and other global developing regions, as rapid dam implementation is evolving on different timescales across the three tributaries.

This research asked the key guiding question: To what extent can satellite remote sensing monitor the hydrologic impacts of dam implementation on SSC in the 3S tributaries? The study objectives were as follows:

- Develop an empirical model for predicting SSC in the 3S basin from satellite remote sensing visible and NIR band data, and demonstrate the skill of the model in resolving seasonal river channel SSC patterns.
- Determine the mechanisms and scales of SSC changes due to dams in their different life-cycle phases, and how impacts on SSC may vary based on reservoir size and location.
- Determine the mechanisms and scales of SSC changes due to other landscape impacts, which are gathered from satellite remote sensing land cover and nighttime light data.
- Assess how SSC changes due to compounding dam and landscape development in the 3S basin have impacted the SSC of the Mekong River mainstem.

This work provides practitioner and hydrologic engineering-oriented understanding of the strengths and limitations in using satellite remote sensing for the above objectives. The methods and results are relevant to the broader MRB as well as other global river basins undergoing rapid dam and landscape development with limited capacity for in situ monitoring.

The Background section provides background on the 3S basin and the technique for estimating SSC using satellite remote sensing data. Data and Methods provides an overview of the in situ and remote sensing data used as well as the methods for analyzing SSC patterns in the study area. The paper ends with Results and Discussion, and a summary of conclusions for suggested improvements and future research directions.

Background

3S Basin

The 3S basin is approximately 78,650 km^2 in area, which is ~10% of the total MRB area (795,000 km^2). Annual rainfall over the 3S basin varies from 1,100 to 3,800 mm (Piman et al. 2013). The climate is monsoonal, and approximately 80% of annual runoff occurs during the monsoon season, June through November (Wild and Loucks 2014). Mean annual streamflow discharge of the 3S is ~2,890 m^3/s, which is ~20% of the Mekong River's ~15,000 m^3/s mean annual discharge (MRC 2005; Adamson et al. 2009). Mean annual suspended sediment load of the 3S, estimated from limited in situ data, is in the range of $\sim 10 - 25$ million $ton/$year. This range is ~6%–16% of the Mekong River's suspended sediment load of ~160 t/year (Sarkkula et al. 2010; ICEM 2010).

Estimating SSC from Satellite Remote Sensing Imagery

Approaches for estimating SSC from satellite remote sensing are generally either empirical or physics based (Wackerman et al. 2017). An empirical approach was used in this study because there are insufficient 3S basin sediment data available to properly parameterize physics-based models. The empirical approach was a regression between in situ SSC and remote sensing visible and NIR data collected for the same location and day. This technique was used because of its simplicity and widespread application. More advanced empirical techniques include nonlinear multiple regression, principle components analysis, and neural networks (Gholizadeh et al. 2016).

Linear regression techniques for estimating SSC have commonly used the visible (red, green, blue) and NIR bands of the Landsat satellite series (TM, ETM+, OLI) to correlate to in situ SSC measurements (Gholizadeh et al. 2016). Regression was conducted between in situ measurements and a single band or band ratio, with the values in linear or exponential form. The red band (alone or in a ratio) was used most often. Using band ratios was more robust than using single bands, particularly when sediment color varies (Pavelsky and Smith 2009). Regression relationships have typically been exponential, linear, or second-order polynomial (higher order polynomials often overfit). Exponential relationships have often been strongest, particularly for high SSC (>50 mg/L) (Pavelsky and Smith 2009; Wackerman et al. 2017).

There are notable limitations and sources of uncertainty in developing and applying the linear regression technique for estimating SSC from satellite visible and NIR surface reflectance data. River sediment properties (e.g., color, mineralogy, grain size distribution) can vary across a region and over time. This can limit the spatial and temporal applicability of empirical SSC-reflectance relationships (Pavelsky et al. 2009). Other reflective suspended or dissolved material (e.g., chlorophyll, carotenoids) can also alter river surface reflectance and therefore the validity of calibrated relationships (Wackerman et al. 2017). Another limitation comes from the penetration depth of satellite sensors for surface reflectance of water (top ~1–2 m). When the river bottom is shallower than the sensor penetration depth, it will scatter the remote sensing reflectance (Volpe et al. 2011). When the river bottom is deeper than the sensor penetration depth, the SSC measured in the surface layer may significantly differ from the depth-integrated SSC. This latter case is likely to occur at high discharges, when bedload and coarser sediment in the lower water column may be a higher proportion of the total load. Thus, SSC predicted from remote sensing cannot be directly used for depth-integrated SSC analyses and modeling. Furthermore, it is not possible to differentiate if increases in remotely sensed SSC are resulting from suspended sediment increases in the entire water column or from mixing between the lower and upper water columns (Markert et al. 2018).

The temporal extent and frequency of remote sensing imagery can also limit its capacity to monitor SSC (e.g., 8- or 16-day revisit interval for Landsat; Sentinel-2 available since 2014). Imagery quality may be limited due to cloud cover. This issue is prevalent in the 3S basin due to its monsoonal hydroclimatology and moutainous landscape, which lend to orographic lift and cloud development. Hence, it is generally appropriate to rely on remote sensing for monitoring background seasonal SSC rather than isolated events (Wackerman et al. 2017). In addition, seasonal SSC from dry, noncloudy seasons is more reliable than that from wet, cloudy seasons. The spatial resolution of remote sensing imagery (e.g., 30 m for Landsat) can also limit the use of satellite remote sensing for sediment. The stream locations where SSC can be monitored must have river channels wide enough so that there are sufficient remote sensing pixels of water that do not mix with the river banks. Narrow channel widths are common for streams with low-orders and steep slopes. These conditions are often found in the uplands of mountainous regions, which are typically large sources of sediment.

Data and Methods

Regression Model for In Situ SSC and Remote Sensing Reflectance

In Situ SSC Data

The in situ SSC data used in this study (Table 1, Fig. 1) were from two Mekong River Commission (MRC) monitoring programs. The data are not publicly available and are the only datasets containing 3S basin SSC samples. The primary dataset was from the water quality monitoring program (WQMP) established by the MRC in 1985 (MRC 2011). As part of the WQMP, MRC member countries monitor SSC throughout the lower MRB. Aside from PK (Mekong, upstream of 3S confluence), the WQMP stations have been monitored for only a subset of years since 1985. The WQMP monitoring is generally monthly, although SSC data have been collected less frequently at some stations. The second dataset was from the MRC Discharge Sediment Monitoring Project (DSMP; Koehnken 2014), which began in 2009. As part of the DSMP, 34 streamflow and SSC samples are collected per year at each site. Channel width and depth measurements at the station locations were obtained using the cross-section tool in Google Earth. Thus, the accuracy and precision of these data were limited and may not represent the channel conditions at satellite and in situ SSC sample collection times.

Although the focus on calibrating the empirical SSC-reflectance relationship was on 3S basin SSC, data from the three Mekong (mainstem) stations within the vicinity of the 3S outlet were incorporated because they provided a larger number of potential calibration samples. The Mekong SSC is generally higher than the 3S, which also extended the range of SSC in the calibration. However, incorporating these stations also introduced more uncertainty to the empirical SSC-reflectance relationship, because the suspended sediment in the mainstem and 3S basin may have different properties. Uncertainty is also induced by different channel geometry conditions where stations are located, which can be broadly grouped between the mainstem and SKB (Sekong River at bridge) stations, upper tributary stations, and lower tributary stations (Table 1, column 4).

The WQMP samples were collected at shallow depths (0.3–0.5 m below water surface) in the middle of the active channel (MRC 2013; Walling 2008). The samples were also collected from a bottle rather than specialized sampling equipment for depth-integrated SSC measurements. The sampling techniques used may have caused deficiencies in sample quality because the samples were not isokinetic (i.e., streamflow at sampler intake may be changing in velocity). Also, given that SSC typically increases with depth, the shallow SSC samples likely underestimated the mean cross-section SSC (Walling 2008). However, the shallow depths of the MRC observations were comparable with the shallow depth observed from remote-sensing sensors (Markert et al. 2018). The DSMP samples were collected with a D-96 sampler for all samples except those collected at PK, where the bottle-sampling approach for the WQMP was used. The D-96 sampler collected depth-integrated and isokinetic samples (Federal Interagency Sedimentation Project 1941), and thus mitigated the limitations of the WQMP samples. Although there were limitations in comparing the bottle and D-96 samples, none of the D-96 samples were used for calibrating the empirical SSC-reflectance relationship because they did not temporally coincide with satellite imagery.

Remote Sensing as the Water Management Tool

Satellite remote sensing data used in this study were from the Landsat satellite series; that is, Landsat TM (Landsat 4 and 5), ETM+ (Landsat 7), and OLI (Landsat 8). Collectively, these satellites have been operational from 1982 to present (Landsat 4: 1982–1994, Landsat 5: 1984–2012, Landsat 7: 1999–present, Landsat 8: 2013–present). Each satellite had a sun-synchronous orbit and 16-day revisit orbital, with an 8-day offset between any two satellites that had overlapping operational periods. Landsat had a spatial resolution of 30 m for the visible (red, blue, green) and NIR wavelengths. Landsat imagery was downloaded and processed using Google Earth Engine (GEE), a cloud-based remote-sensing platform.

Table 1. Information on in situ monitoring stations and SSC samples of the 3S basin and Mekong River mainstem used in this study

Station name	Station abbreviation	Source	Tributary/location	SSC sampling start date	SSC sampling end date	Number of SSC samples	Channel top width (m)	Channel depth (m)
Siempang	SP	WQMP	Sekong, lower	10/24/2004	8/25/2011	65	303	3.7
Kontum	KM	WQMP	Sesan, upper	10/15/1992	3/15/1995	34	104	1.0
Trung Nghia	TN	WQMP	Sesan, upper	6/15/1992	3/15/1995	35	61	4.8
Pleicu	PU	WQMP	Sesan, upper	7/15/2004	8/15/2011	81	203	11
Phum Pi	PP	WQMP	Sesan, upper	11/23/2004	2/26/2011	43	173	3.0
Andaung Meas	AM	WQMP	Sesan, lower	11/23/2004	6/27/2011	66	286	4.0
Giang Son	GS	WQMP	Srepok, upper	9/15/1993	2/15/1995	26	53	<1
Duc Xuyen	DX	WQMP	Srepok, upper	11/15/1992	2/15/1995	84	101	<1
Ban Don	BD	WQMP	Srepok, upper	10/15/2004	5/15/2011	84	120	2.0
Lumphat	LT	WQMP	Srepok, lower	11/23/2004	2/27/2011	66	350	8.5
Pakse	PK	DSMP	Mekong, upstream	6/17/2011	3/25/2015	92	1,615	3.9
		WQMP	of 3S confluence	12/18/1985	6/17/2011	267		
Stung Treng	ST	DSMP	Mekong, downstream	6/8/2011	9/30/2014	83	1,376	4.3
		WQMP	of 3S confluence	12/18/2004	2/26/2011	65		
Kratie	KT	DSMP	Mekong, downstream	6/7/2011	9/29/2014	74	1,108	8.0
		WQMP	of 3S confluence	12/19/1995	12/28/2011	160		
Sekong River at bridge	SKB	WQMP	3S confluence	8/11/2012	9/30/2014	52	812	4.1

Sources: Data from MRC (2011); Koehnken (2014).
Note: WQMP = water quality monitoring program; and DSMP = discharge sediment monitoring project.

Landsat collections of precomputed surface reflectance with the highest quality rating (Tier 1) were used. These scenes available in GEE have been atmospherically corrected and have mapped pixels of cloud, cloud confidence, cloud shadow, and snow/ice [see Markert et al. (2018) for more information]. Landsat 4 data of Tier 1 quality were sparsely available in the 3S basin. Landsat 7 data are of limited availability since 2003, when a failure of the scan line corrector occurred (Chander et al. 2009).

Satellite visible and NIR reflectance data were collected at each in situ monitoring station location over a stream reach roughly three times as long as the stream width (Fig. 1). Surface water pixels over the stream reach were mapped using the dynamic surface water extent algorithm (Jones 2015). Pixels with clouds or cloud shadows were masked out using the Landsat quality assessment bands. Scenes were retained if they contained at least 90% of pixels classified as being free of clouds and cloud shadows over the sample reach. Scenes were excluded if the average NIR reflectance was greater than 0.5 because they were likely to have severe cloud contamination. The remaining image collections were manually inspected, and scenes were excluded if a significant portion of pixels were impacted by clouds, cloud shadows, haze, and/or patches of sand.

Satellite data for 12 of the 14 in situ monitoring stations were used in this analysis. Data from GS (Srepok) and TN (Sesan) were excluded because the narrow river widths limited the number of surface water pixels at these locations. Satellite data were also used from six locations in the study area that are not in situ monitoring points (Fig. 1). This resulted in a total of 4,556 images combined for the 18 monitoring points (12 in situ points, 6 non-in-situ points). Of these images, 1,355 (30%) were from the wet season and 3,201 (70%) were from the dry season.

Empirical Model Development and Application

A calibration dataset was developed to test for correlation between the in situ SSC and satellite reflectance data. The calibration dataset consisted of all quality-checked Landsat data collected on the same date and location as an in situ sample. This amounted to a total of 15 corresponding in situ and Landsat samples, coming from 10 of the in situ monitoring points (Fig. 2, bottom left). Of the corresponding samples, eight were collected during the dry season and seven during the wet season. In addition to the limitations for the in situ data previously discussed (see the section, In Situ SSC Data), the calibration dataset was limited because of its small number (n = 15), only two of the in situ observations are greater than 60 mg/L, and 9 of the 15 calibration pairs come from four locations. These factors limited the precision of SSC values predicted from the empirical model, particularly for high SSC. However, the range of the calibration dataset was acceptable given that the maximum observed SSC value in the calibration dataset (153 mg/L) is the 97th percentile of all in situ observations in the 3S basin. The empirical model was also biased toward locations/rivers from which more calibration data were obtained. However, each of the three tributaries and the mainstem were represented in the calibration dataset.

Using the calibration dataset, empirical regression models were tested between the in situ SSC and satellite reflectance data. Reflectance data were tested as individual visible (red, blue, green) and NIR band values as well as all permutations of band ratios (e.g., red/green, blue/NIR). The SSC and reflectance values were tested in linear and exponential forms with exponential, linear, and second-order models. Exponential models had the best coefficient of determination (r^2) and root mean square error (RMSE) metrics between the SSC observed in situ and the SSC predicted from the empirical regression model with satellite data. Of the different bands and band ratios correlated with in situ SSC, the best fit was the red band ($r^2 = 0.78$, RMSE $= 21.2$ mg/L; Fig. 2). The band ratios between red and the other three bands had relatively strong and similar performance ($r^2 = 0.63$–0.66, RMSE $=$ 26.3–27.6 mg/L; Fig. 2).

When the calibrated red band SSC equation was applied to time series of red reflectance at in situ monitoring stations, peak values of predicted SSC tended to be anomalously high. When the red/green, red/blue, and red/NIR calibration equations were applied to the respective reflectance time series at stations, peak values predicted by the red/green band SSC equation did not have high anomalies and were closest to observations. Hence, the final empirical model conditionally used the red (R) and red/green (R/G)

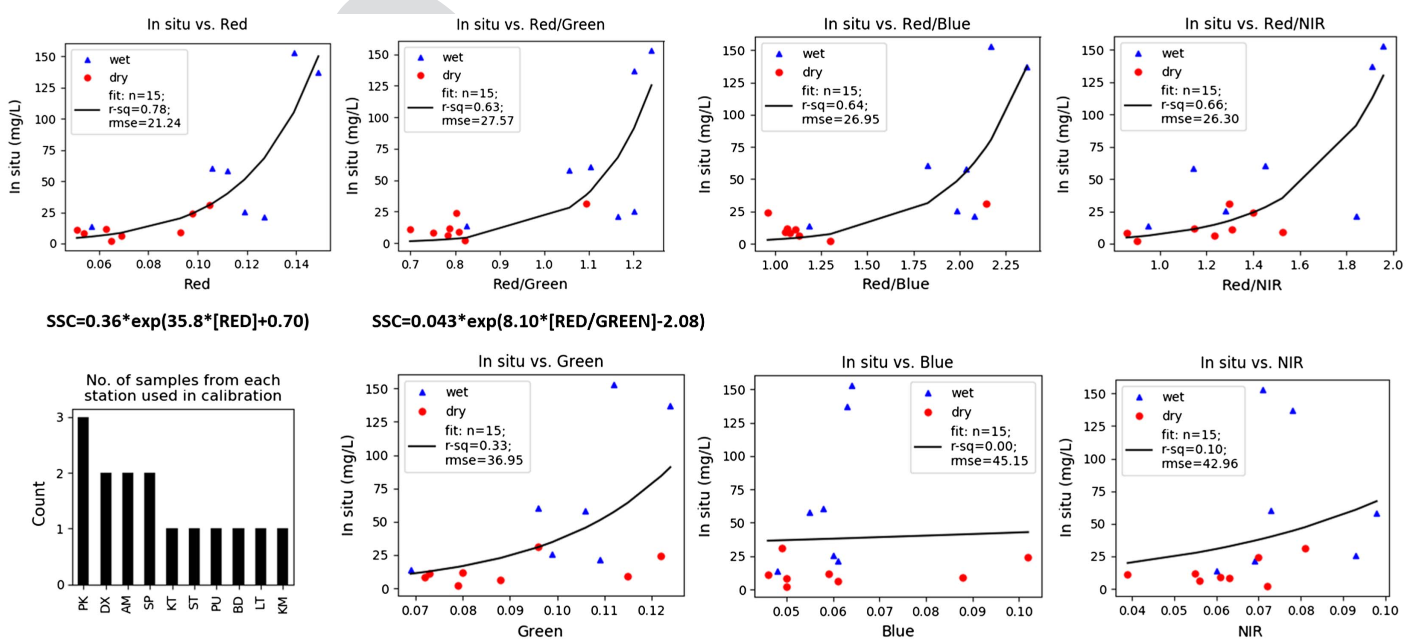

Fig. 2. Regression results for in situ observations of SSC versus remote sensing reflectance for a single band or band ratio.

calibration equations: For R less than 0.14, the red band SSC equation was applied; for R greater than or equal to 0.14, the R/G band ratio SSC equation was applied. In equation form, this is

$$\begin{aligned} \mathrm{SSC} &= 0.36 \times \exp(35.8 \times R + 0.70) \quad R > 0.14 \\ \mathrm{SSC} &= 0.043 \times \exp(8.10 \times R/G - 2.08) \quad R \leq 0.14 \end{aligned} \tag{1}$$

The red reflectance threshold of 0.14 in the empirical model was determined through sensitivity testing. The monthly mean SSC from the empirical model was computed for a range of plausible thresholds (red = 0.10–0.17) and the results were compared to the monthly mean in situ SSC at each monitoring station. While the optimal red band threshold varied across stations, the threshold 0.14 performed best overall for SP (Sekong), AM (Sesan), and LT (Srepok). Optimizing model performance at these three stations was prioritized because they are closest to the outlet of each 3S watershed. The empirical model captured the general seasonal patterns and magnitudes of the in situ observations at the three stations, although there was still uncertainty for high SSC (Fig. 3). The empirical model improved the monthly mean SSC prediction at AM (RMSE declined from 393 to 65.5 mg/L), and LT (RMSE declined from 50.7 to 23.6 mg/L), however, had no change at SP (RMSE of 43.7 mg/L).

To develop long-term time series of predicted SSC for all monitoring stations, the empirical model was applied to all quality-checked Landsat surface reflectance data. The time series of instantaneous SSC predictions were smoothed using the locally weighted scatterplot smoothing technique (LOWESS; Cleveland 1979). This robust, nonparametric technique was suitable for the non-equally-spaced temporal frequency of the surface reflectance data. For each predicted value, a specified fraction of the dataset adjacent to the output was smoothed, with more weight given to points closest to the predicted value. The specified fraction was determined through sensitivity testing to be 0.07, as this preserved the seasonality of the data while limiting the noise.

Data on Dams, Land Cover, and Nighttime Lights

Dams

The primary source of information on dams in the 3S basin was a dataset maintained by the CGIAR Research Program on Water, Land, and Ecosystems (WLE 2017). The dataset was intended to contain every MRB hydropower or multiuse dam with an installed capacity of 15 MW or higher, and/or every irrigation or water supply dam with a reservoir area of 0.5 km^2 or larger. Additional information on 3S basin dams was obtained from the studies of Schmitt et al. (2018), Piman et al. (2016), and Wild and Loucks (2014), which all focused explicitly on dam impacts in the 3S basin. These three studies included information from the MRC dam database, which is not publicly available. Each study also included calculations made in the respective analysis for relevant properties of the dams (e.g., drainage area).

Of the 65 dams existing, under construction, or planned in the 3S basin, 14 existing dams were the focus of this study (hereinafter referred to as focus dams; Table 2). These focus dams were expected to have the greatest impact on the 3S sediment regime, largely based on their reservoir volume, surface area, and/or drainage area. Findings from other studies on the hydrologic impacts of 3S basin dams were also considered. Three sets of dams were grouped together in this analysis due to their spatial proximity and similar construction timelines: Sesan 3 and Sesan 3A; Sesan 4 and Sesan 4A; and Srepok 3 and Srepok 4. In addition, Xepian-Xenamnoy dam construction was considered in this analysis, although this dam collapsed in June 2018.

Detailed construction information about the MRB dams is typically not publicly available. Thus, to understand how different dam

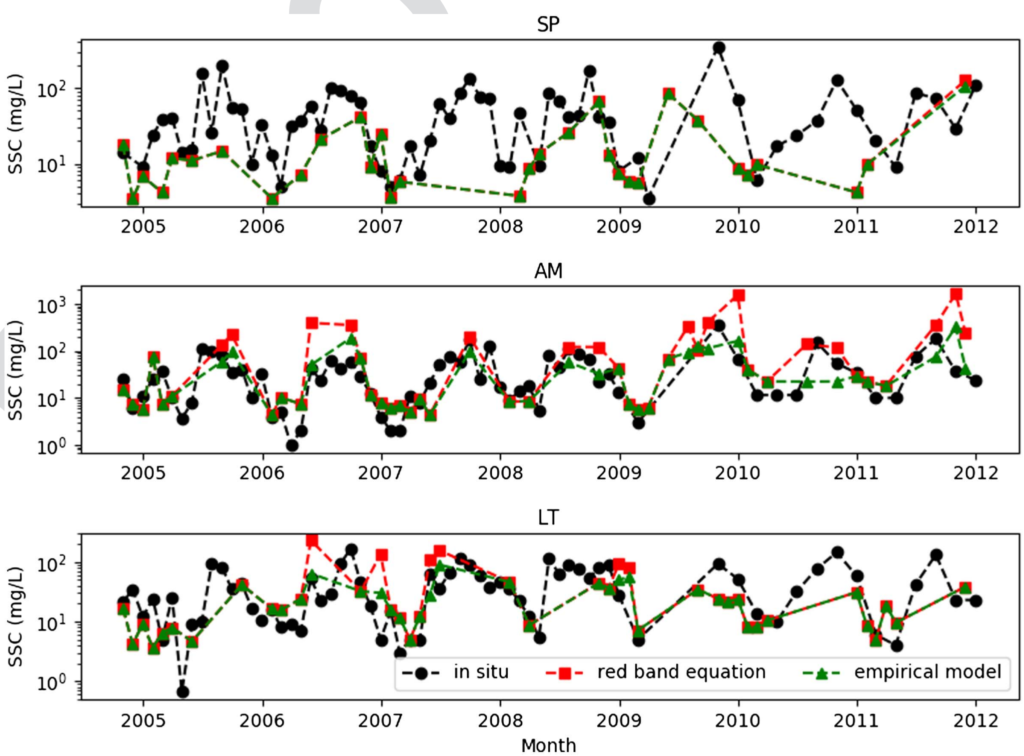

F3:1 **Fig. 3.** Time series of in situ and predicted monthly mean SSC at SP (Sekong), AM (Sesan), and LT (Srepok). Predictions are shown for both
F3:2 calibrated red band SSC equation and empirical model, which uses the red band SSC equation and red/green bands SSC equation.

12 **Table 2.** Dams in 3S basin studied for sediment impact

T2:1	Name	Basin	Commiss-ioning date	Installed capacity (MW)	Drainage area (km^2)	Max reservoir surface area (km^2)	Total storage (million m^3)
T2:2	Houayho	Sekong	1999	152	192[a]	37	674[b,c]
T2:3	Xekaman 1	Sekong	2015	290	3,580[a]	150	4,804
T2:4	Xepian-Xenamnoy	Sekong	2019	410	522[a]	50	1,092
T2:5	Yali	Sesan	2001	720	7,455[a]	64.5	1,073
T2:6	Sesan 3	Sesan	2006	260	7,788[a]	6.4	92[b,c]
T2:7	Sesan 3A	Sesan	2007	96	8,084[a]	8.8[b]	80.6[b,c]
T2:8	Plei Krong	Sesan	2008	100	3,216[a]	53.3	1,049
T2:9	Sesan 4A	Sesan	2008	63	9,368[a]	1.8	13.1
T2:10	Sesan 4	Sesan	2009	360	9,326[a]	54	893.3
T2:11	Buon Trah Srah	Srepok	2009	86	2,930[a]	37.1[b]	787[b,c]
T2:12	Buon Kop	Srepok	2009	280	7,980[a]	5.6[b]	73.8[b,c]
T2:13	Srepok 3	Srepok	2009	220	9,410[a]	17.7[b]	219
T2:14	Srepok 4	Srepok	2009	80[a]	9,568[a]	3.8[b]	29.3[b,c]
T2:15	Lower Sesan/ Srepok 2	Sesan, Srepok	2017	480	49,200[a]	335	1,790

13 Source: Data from WRE (2017) unless indicated.
[a]Data from Piman et al. (2016).
[b]Data from Schmitt et al. (2018).
[c]Data from Wild and Loucks (2014).

lifecycle phases impacted SSC, Landsat imagery was manually reviewed to approximate when dam construction began and initial reservoir filling was complete for each of the 14 focus dams. The approximate dates obtained were the dates when relevant Landsat imagery was available and not necessarily the actual date that the milestone occurred. The accuracy of the dates was limited due to imagery availability, clouds covering the dam/reservoir in the imagery, and potential misinterpretation of the imagery. This, in turn, could have caused misinterpretation of dam construction and operation impacts on SSC in the results of this study. However, the dates are expected to be accurate within $+/-1$ year, which is minor compared to the long time frame of this study (~31 years) and, typically, multiyear SSC trends.

The bulk of dam development has occurred differentially among the 3S basins (Table 2). In the Sesan basin, major development began primarily in 2006, although a large dam (Yali) was also constructed in 2001. Major development followed in the Srepok basin, beginning in 2009. Finally, major development began in the Sekong basin in 2015, although a large dam (Houayho) was constructed in 1999.

Land Cover

14 Land cover data across the 3S basin were obtained from the Moderate Resolution Imaging Spectroradiometer (MODIS) Aqua and Terra Land Cover Product (MCD12Q1 V6; NASA, Washington, D.C.) and supervised land cover classification of this MODIS data from the International Geosphere-Biosphere Programme (IGBP; Loveland and Belward 1997; Belward et al. 1999). The data were produced at 500-m spatial resolution and annual time steps for years 2001 to 2017 ($n = 17$). There were 12 land cover classifications found in the 3S. In this study, classifications were grouped into categories as follows: forest includes evergreen broadleaf forests, deciduous broadleaf forests, and mixed forests; savanna includes savannas and woody savannas; cropland includes croplands and cropland/natural vegetation mosaics. The remaining land cover classifications were grassland, wetland, barren, water bodies, and urban.

Nighttime Light

Nighttime light data were used in this analysis as a proxy for human settlement dynamics (Fig. 4), as done in other studies (e.g., Mård et al. 2018; Xu et al. 2014). Human settlement dynamics reflect potential nonpoint sources of river sediment. Nighttime light data were a helpful complement to land cover data in the 3S basin given that the region is largely rural, and concentrated human settlement is not always apparent or quantifiable from land cover data. Nighttime light data across the 3S basin came from the Defense Meteorological Satellite Program Operational Linescan System (Version 4) (NOAA–Earth Observation Group 2016). These data were produced at 30 arc second (~1 km) spatial resolution and annual time steps for years 1992 to 2013 ($n = 22$). However, the start year of 2001 was used in Fig. 4 for consistency with the land cover dataset temporal range. There was little increase in nighttime lights from 1992 to 2001 in the study area. In this study, "stable" nighttime light data were used, which quantify light intensities from cities and towns, excluding background noise (e.g., sunlit data) as well as temporary light sources (e.g., fires) (Mård et al. 2018). Nighttime light units ranged from 0 (complete darkness) to 63 (bright areas). 15

Results and Discussion

In the predicted SSC time series at each monitoring point [Figs. 5(a), 6(a), 7(a), and 8(a–c)], there were frequent satellite data gaps beyond the 8- or 16-day Landsat revisit intervals (which would be ~45 or ~22 points per year). Data gaps were prevalent in the wet season when clouds were a common issue. Thus, remote sensing reflectance data were mostly from the dry season (74% at SP, 69% at AM, and 77% at LT), causing the dry season SSC to dominate the LOWESS-smoothed SSC patterns. SSC was generally lower and less variable in the dry season compared to the wet season. There were also exceptionally long periods where data were sparse in both the wet and dry seasons, such as 2010 to 2013 at SP [Fig. 5(a)]. In these periods the LOWESS-smoothed SSC time series may have been biased, particularly by anomalously high or low SSC predictions.

Although the LOWESS-smoothed SSC time series [Figs. 5(a), 6(a), 7(a), and 8(a–c)] were impacted by biases, they show insightful changes in response to dam and landscape development [Figs. 5(b and c), 6(b and c), 7(b and c), and 8] over the ~31 year period analyzed. In the initial ~17 years (until ~2004/2005) of the SP, AM, and LT time series, the SSC were generally at relatively low (<10 mg/L for SP and AM; <20 mg/L for LT) and stable

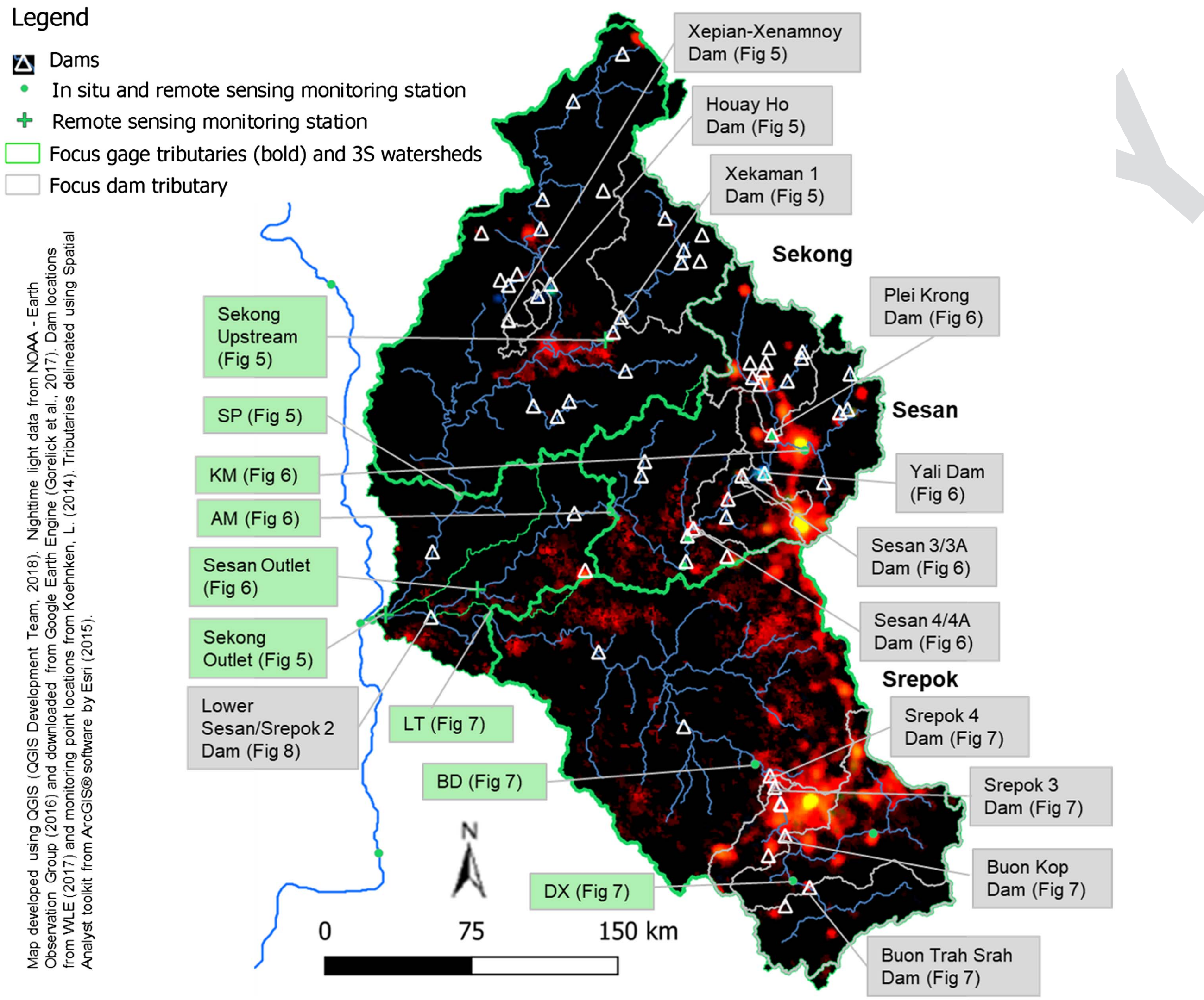

Fig. 4. Stable nighttime light trends in 3S basin from 2001 to 2013. Increasing red intensity indicates an increasing nighttime light trend; increasing blue intensity indicates a decreasing nighttime light trend; black indicates no trend; yellow indicates locations where brightness was initially high (i.e., trend offset) and has an increasing trend. [Map developed using QGIS (QGIS Development Team 2018). Nighttime light data from NOAA–Earth Observation Group (2016) and downloaded from Google Earth Engine (Gorelick et al. 2017). Dam locations from WLE (2017). Monitoring point locations from Koehnken (2014). Tributaries delineated using Spatial Analyst toolkit from ArcGIS software (Esri, Redlands, California).]

baseline values. There were short periods where SSC were slightly elevated due to early, isolated dam construction, such as the Yali dam from 1993 to 1998 [Fig. 6(b)].

For the latter ~14 years (from ~2004/2005 to 2019) in each tributary, there were more dramatic changes in LOWESS-smoothed SSC caused by more extensive dam implementation and landscape development. Reservoirs with larger surface area, volume, and/or drainage area generally had a stronger influence on SSC trends. Dam impacts on SSC also depended on the lifecycle stage of the dam. Temporary increases in SSC occurred at the onset of dam construction [Figs. 5(b), 6(b), and 7(b)], as land surface disturbance from the construction of/related to dams eroded sediment. Because of localized construction impacts, SSC increases were typically higher at points closer to the dam(s) under construction than at downstream points. For example, during Xekaman 1 dam construction [Figs. 5(a and b)], SSC increased by >300 mg/L in the vicinity of the dam and 20–120 mg/L at monitoring points downstream. Overall SSC increases related to dam construction ranged from ~5–120 mg/L at SP, ~20–50 mg/L at AM, and ~3–40 mg/L at LT. The duration until reaching the peak SSC ranged from less than 1 year [Srepok 3 and Srepok 4, Figs. 7(a and b)] to 6 years [Xekaman 1, Figs. 5(a and b)].

As the reservoirs filled, the LOWESS-smoothed SSC declined downstream of the reservoirs due to the lessening of construction impacts as well as the reservoir sediment trapping. For example, in the Sekong watershed [Figs. 5(a and b)], SP declined to baseline SSC (122 to 8 mg/L) within 2 years of when Xekaman 1 reservoir filled. In the Srepok watershed [Figs. 7(a and b)], LT decreased to near baseline conditions (47 to 14 mg/L) within the year that the Buon Trah Srah and Buon Kop reservoirs filled. Sediment trapping by the reservoirs was clearly demonstrated in the Sesan watershed [Figs. 6(a and b)]. When the SSC of KM—the point upstream of all major dams—was most dramatically elevated from 2009 to 2012 (39 to 156 mg/L), the SSC at AM simultaneously declined and remained below 50 mg/L. The difference in SSC between KM and AM was up to 108 mg/L, which is likely due to sediment trapping in reservoirs between the two points. The dams in between KM and AM—Yali, Sesan 3/3A, and Sesan 4/4A— had their reservoirs filled or were in the process of filling during this period.

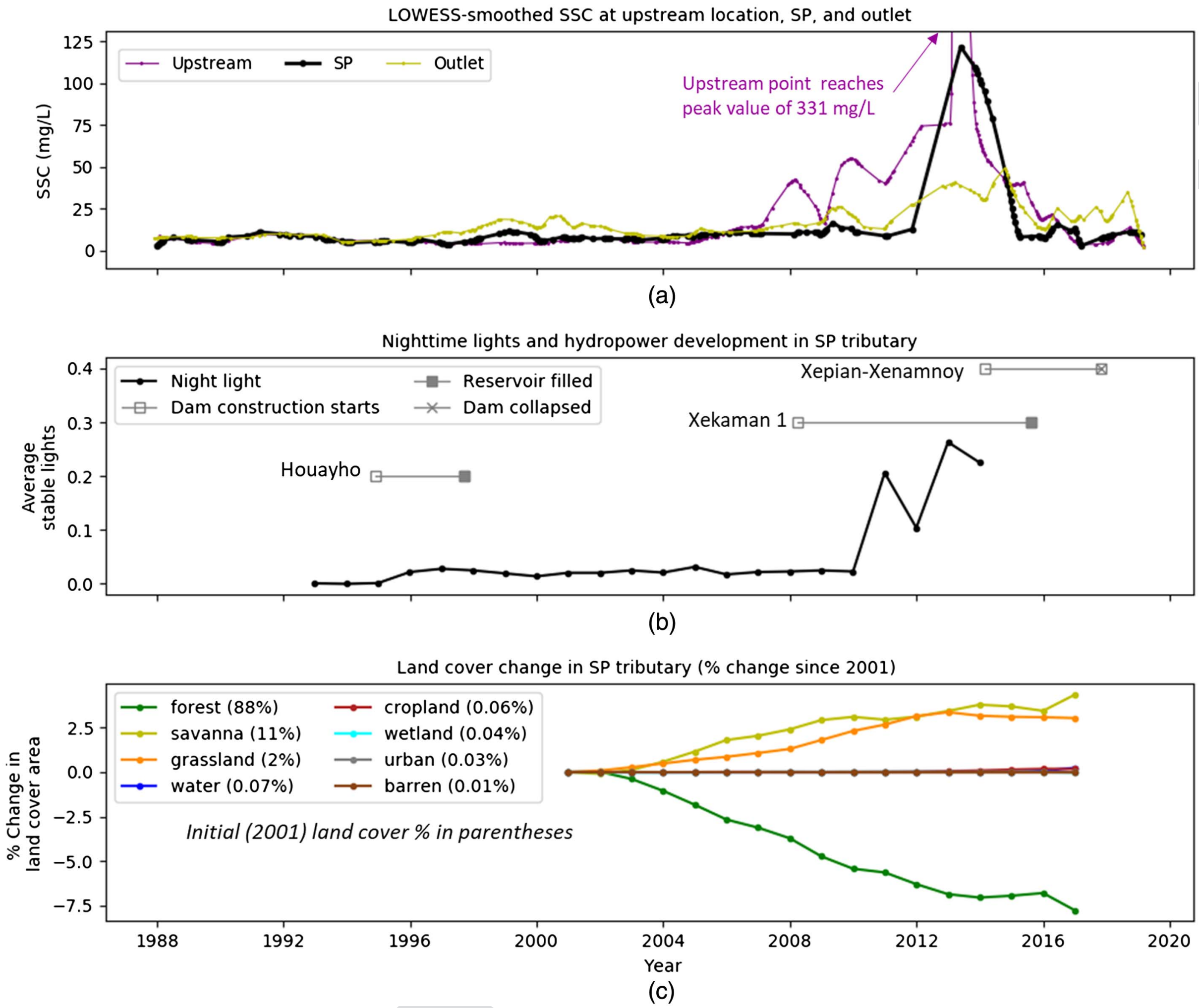

Fig. 5. Time series of: (a) predicted LOWESS-smoothed SSC; (b) dam implementation and nighttime light; and (c) land cover change in the Sekong watershed.

Decreases in SSC typically occurred less rapidly at monitoring points located closer to dams compared to downstream points, which was likely due to persisting localized impacts of dam construction. Relatively high SSC at monitoring points near the dams may have also been due to the scouring impact of the outflow near the dam spillway. This was seen, for example, in the Srepok watershed [Figs. 7(a and b)] from 2008 to 2013, when BD (upstream) remained elevated at ~40 mg/L while LT (downstream) declined to a steady ~13 mg/L.

At these two points in the Srepok watershed [BD, LT; Figs. 7(a and b)], SSC also began to generally increase (with seasonal fluctuations) in 2015. In 2016, SSC peaked to unprecedented levels for LT at 76 mg/L and for BD at 112 mg/L. These increasing SSC patterns were not attributable to upstream dam construction, although the seasonal fluctuations could relate to dam operations. These increasing SSC patterns also diverged from the generally decreasing SSC patterns at DX, located upstream of Buon Kop, Srepok 3, and Srepok 4.

Land Cover and Nighttime Light Impacts on SSC

SSC time series patterns in conjunction with dam development were better understood using nighttime light and land cover satellite data. The prevalent landscape changes over time in all 3S watersheds were increases in human settlement patterns as inferred from nighttime lights [Figs. 4, 5(b), 6(b), and 7(b)] and decreases in forest cover [Figs. 5(c), 6(c), and 7(c)]. Each of these would have reasonably caused increases in SSC, although the increases may have been temporary. Forest clearing could have led to relatively large sediment loads to streams due to impacts of heavy equipment and tree uprooting. After forest clearing, the lack of tree roots holding sediment in place allowed sediment to more readily erode. Subsequent construction, land cultivation, and human settlement on deforested land may have also eroded sediment. However, initial impacts of deforestation on SSC could have lessened over time. When deforested land was replaced with cropland, the impacts of land cultivation may have also contributed to elevating SSC. The installation of surfaces less conducive to erosion (e.g., concrete) may have allowed for increased surface water runoff but less sediment, which could have diluted SSC.

Deforestation and increasing nighttime lights (i.e., human settlement) generally occurred simultaneously with dam development (Figs. 5–7), and thus had compounding impacts. For example, SSC increases that coincided with dam construction may have been exacerbated by landscape changes. These landscape changes were not just coincidental, but often interconnected with dam development. Areas with significant economic development are more likely to have the demand and resources to implement dams; then,

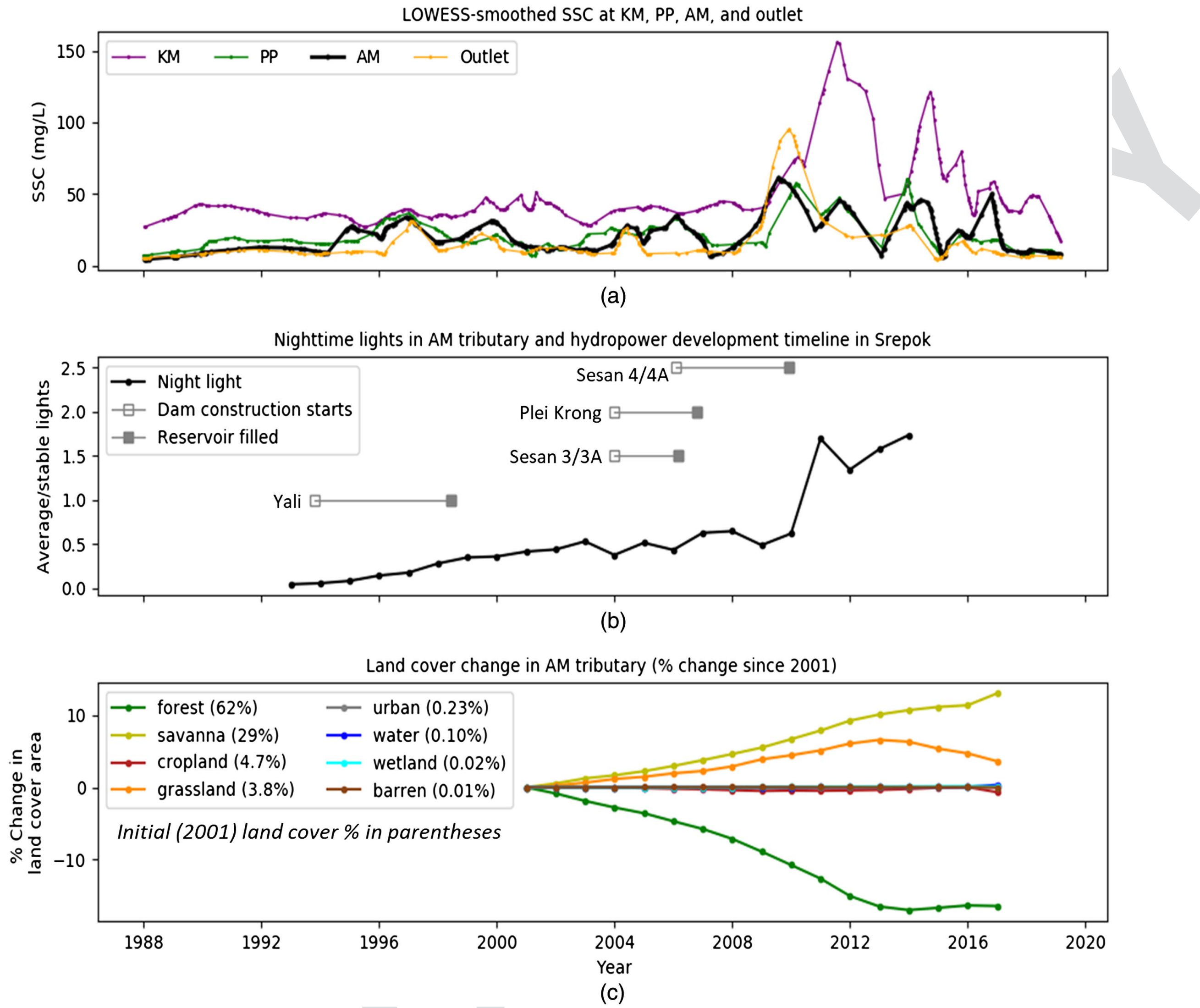

Fig. 6. Time series of: (a) predicted LOWESS-smoothed SSC; (b) dam implementation and nighttime light; and (c) land cover change in the Sesan watershed.

following dam construction, there is further capacity for development in surrounding areas. For example, the magnitude of stable nighttime lights was highest overall in the Sesan and Srepok watersheds [Figs. 6(c), 7(c), and 8(c)]. Areas with initially high nighttime lights (yellow in Fig. 4) and increasing nighttime lights (red in Fig. 4) were most prominent in the Vietnam portions of these two watersheds (Figs. 1 and 4). Vietnam is the most economically developed of the countries spanning the 3S, and the regions of the Sesan and Srepok in Vietnam are also where historic dam development has been most prevalent.

In the Sesan watershed (Fig. 6), KM was in an area of high human settlement that is upstream of dam development (Fig. 4). Thus, the LOWESS-smoothed SSC patterns of KM reflected human settlement and deforestation impacts. The 117-mg/L increase in SSC at KM from 2009 to 2012 coincided with the most dramatic increase (283%) in nighttime lights after 2010 [Fig. 6(b)] as well as decreasing forest cover (−16%) from 2001 to 2013 in the AM tributary [Fig. 6(c)]. The subsequent decline in SSC at KM corresponded to stabilization of deforestation after 2013 [Fig. 6(c)] and nighttime lights after 2011 [Fig. 6(b)]. As discussed above, the dams downstream of KM (Yali, Sesan 3/3A, Sesan 4/4A; cumulative volume of ∼2,152 million m^3) likely trapped suspended sediment, which modulated SSC increases downstream.

In Srepok watershed LT tributary (Fig. 7), there was similarly a dramatic increase (512%) in night time lights after 2010 [Fig. 7(b)] as well as decreasing forest cover (−12%) from 2002 to 2013 [Fig. 7(c)]. Human settlement patterns (Fig. 4) were concentrated just upstream of the Srepok 3 and Srepok 4 reservoirs and BD. Like at KM in the Sesan tributary, the dramatic increase in SSC at BD and LT after 2016 was likely related to the upstream landscape development activities. The downstream Srepok 3 and Srepok 4 dams may have modulated SSC increases prior to 2016. However, the cumulative volume of these dams (248 million m^3) was much lower that of the dams downstream of KM (in Sesan). This may help to explain why the Srepok 3 and Srepok 4 reservoirs were less effective at trapping sediment over time.

Impacts of 3S Basin on Mekong River Mainstem SSC

The impact that the each of the 3S rivers had on the SSC of their junction, SKB, as well as on the Mekong River mainstem, varied between the 3S rivers and over time (Fig. 8). SKB increased most

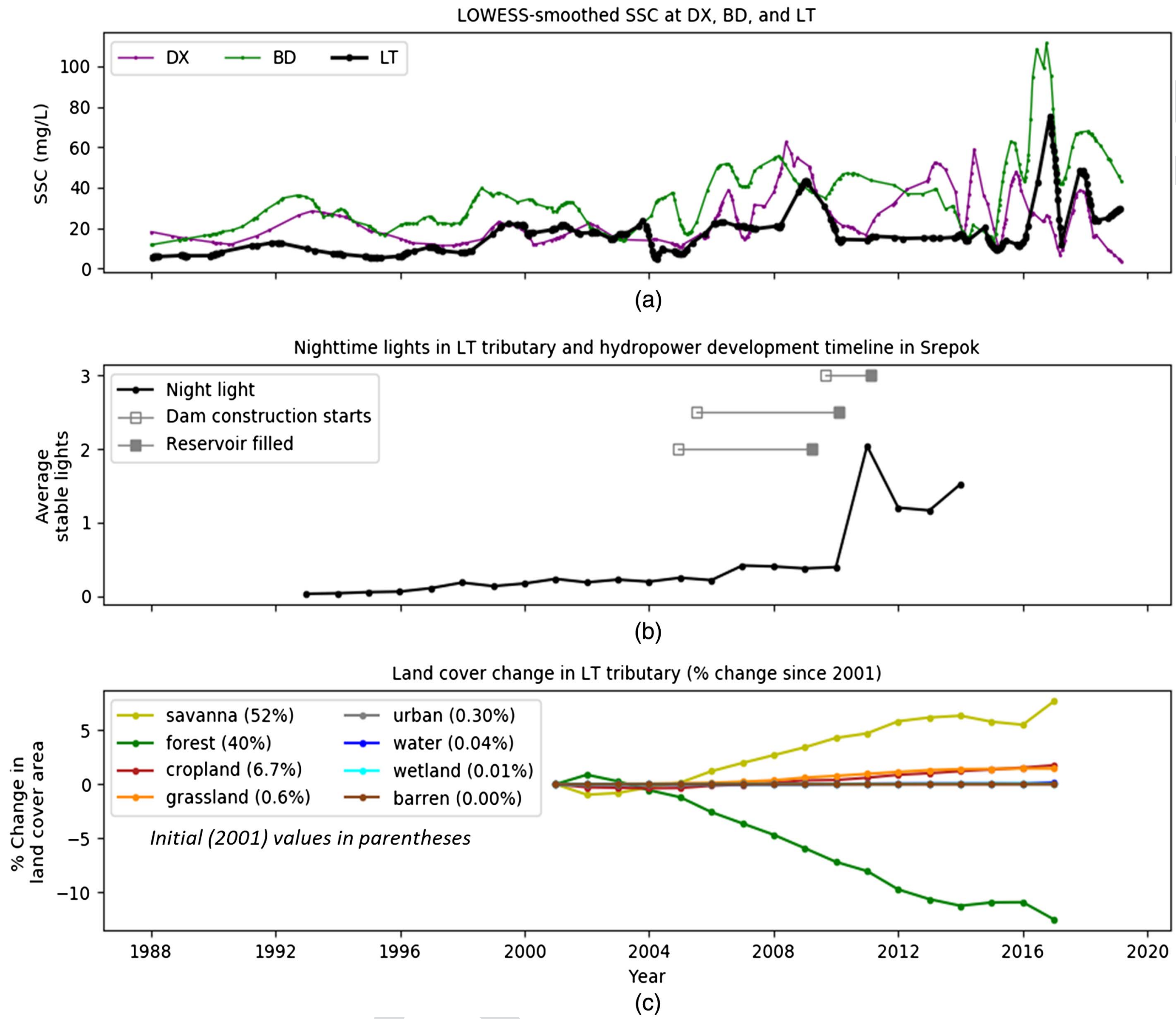

Fig. 7. Time series of: (a) predicted LOWESS-smoothed SSC; (b) dam implementation and nighttime light; and (c) land cover change in the Srepok watershed.

dramatically (peak of 70 mg/L) from early 2007 to early 2009, which coincided with elevated SSC from the Sesan and Srepok outlets [peak of 118 mg/L; Figs. 8(a and b)]. When the Sekong outlet SSC elevated up to 50 mg/L from 2011 to 2017 [Fig. 8(b)], the SKB SSC continued to decline from its 2009 peak, although less rapidly. The SKB SSC temporarily elevated by ~20 mg/L from 2016 to 2018 during construction of the Lower Sesan 2 dam and when SSC was elevated to ~50 mg/L at the Sesan/Srepok outlet. However, it then decreased to <8 mg/L after the Lower Sesan/Srepok 2 dam reservoir filled, likely due to sediment trapping.

Compared to the Mekong SSC, the SKB SSC was relatively low prior to 2007 [Fig. 8(c)]. When the Mekong SSC dramatically peaked in 2000 and 2001, there was up to 125 mg/L difference between SKB and the combined Mekong and 3S SSC (or SKB SSC being ~13% of Mekong SSC). As the Mekong SSC subsequently declined and SKB SSC dramatically elevated starting in 2007, the SKB SSC was up to 35 mg/L greater (100%) than the combined Mekong and SKB SSC in 2010. However, the SKB SSC then continued to generally decline and had diminishing influence on the Mekong SSC—except from 2016 to 2018, when the spike in SKB SSC temporarily elevated the combined Mekong and 3S SSC from 10 to 44 mg/L.

These patterns demonstrate that the Mekong mainstem, like the 3S basin, has had temporary increases in SSC due to dam and landscape development impacts upstream. However, over the past two decades, the SSC of the Mekong has repeatedly reached exceptionally low levels due to upstream reservoir trapping as well as other natural and anthropogenic (e.g., aggregate mines) influences on sediment (Kondolf et al. 2018). The temporary increases in SSC of the 3S due to dam development and landscape change have modulated the decline in SSC of the Mekong. However, as dam building and operations in the 3S basin continue, its contribution of sediment to the Mekong will continue to decline, likely to unprecedented levels.

Conclusion

This study demonstrated that satellite remote sensing is a practical management tool to use for detecting the hydrologic impacts of dam development on SSC at the subbasin scale (3S basin) of the MRB. The capacity of satellite remote sensing for broad temporal and spatial comparison of SSC patterns in subbasins allowed for refined understanding of where and when dams and landscape

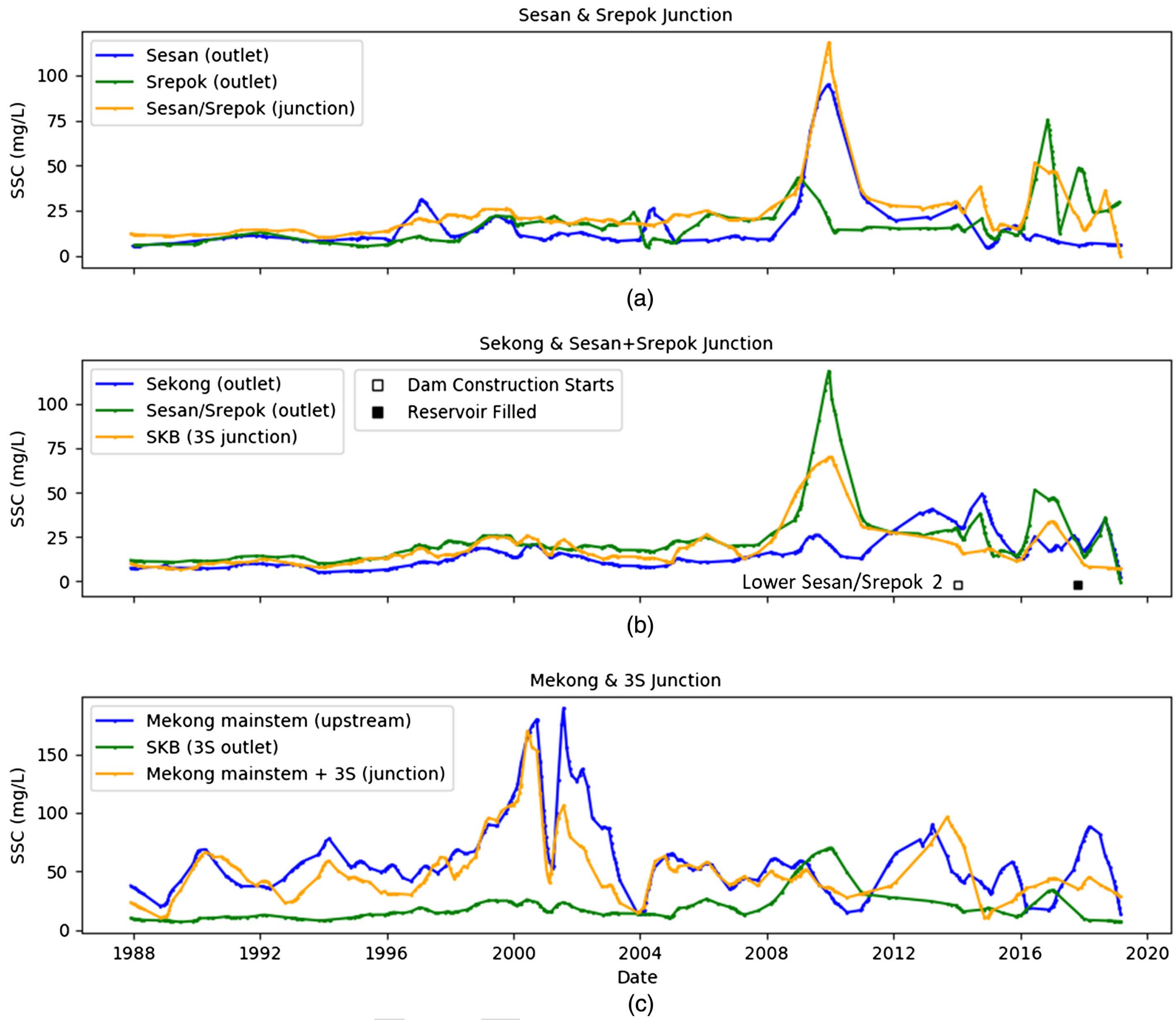

Fig. 8. Time series of: (a and b) predicted LOWESS-smoothed SSC at the outlets and junctions of the 3S watersheds; and (c) the 3S basin and the Mekong mainstem.

changes influenced SSC patterns. This understanding is a critical step toward improved sediment monitoring and adaptive management throughout the MRB. This study showed the capacity of satellite remote sensing to monitor dam and landscape change impacts on SSC as follows:

- Satellite remote sensing was primarily suitable for monitoring background seasonal sediment loads. Dry-season SSC patterns tended to dominate long-term time series because more remote sensing data were available in the dry season due to lack of cloud cover.
- The performance of empirical models in predicting SSC from visible/NIR band data was improved by using separate equations for low (red band) and high (red/green band ratio) SSC. For monthly mean SSC predictions, the RMSE decreased (improved) up to 328 mg/L.
- The remote sensing technique detected changes in SSC due to dam construction (e.g., +120 mg/L at SP) and reservoir sediment trapping (e.g., −108 mg/L between KM and AM).
- Satellite data on nighttime lights, which reflect human settlement patterns, and land cover helped to better explain SSC patterns. Deforestation and increasing human settlement caused SSC increases (e.g., +117 mg/L at KM). The extent to which reservoir sediment trapping downstream of landscape impacts modulated SSC increases depended on reservoir size.
- The technique demonstrated how the SSC of the 3S rivers compared to that of the Mekong mainstem over time (e.g., from ~13% to 100% greater). SSC changes will continue with ongoing dam and landscape development in the MRB, and thus SSC monitoring will be imperative for effective sediment management.

A primary limitation of this work was the precision of the SSC predicted by the empirical model. The calibration of the empirical model introduced large uncertainty due to the small number of data ($n = 15$), a low number of high SSC (<60 mg/L) data values ($n = 2$), unequal distribution of the monitoring stations from which data were obtained, and different sediment properties and channel conditions for the different monitoring stations. The wet-season SSC predictions are also sparse due to high cloud cover and may be biased, particularly by anomalously high or low SSC predictions. Hence, future work should involve collecting and integrating additional in situ and satellite data, including data from other satellites (e.g., Sentinel-2). Further research on the river basin geomorphology and sediment properties (e.g., mineralogy) may also aid in improving the empirical model, and more complex techniques (e.g., neural networks) can be explored. Additional factors that influence sediment dynamics, such as climate and other human interventions, can also be integrated to improve this work and similar applications. The workflow for the approach used would be expedited and more reliable with improvements to Landsat could masking techniques.

While there are limitations in the data, techniques, and scope of this work, it should not hinder practitioners from leveraging the information that satellites can provide in better informing river, dam, and sediment management. The information that satellites provided in this study and similar applications offers first-order system understanding, which can inform researchers where additional localized investigations should be conducted. The approach used can be implemented for ongoing monitoring and analysis of SSC in the MRB and other global river basins undergoing dam development and landscape changes. Findings from this work and future applications can also inform hydrologic engineers or water managers where and how suspended sediment impacts can be managed and mitigated. Furthermore, methods and results of this work can be used synergistically with computational modeling (e.g., Wei et al. 2019) and additional remote sensing data (e.g., precipitation) to address related scientific, engineering, and management questions. Overall, satellite remote sensing is shown in this study to be an effective tool for understanding dam impacts to suspended sediment on broad spatial and temporal scales. It can help to address critical needs for improved sediment monitoring, adaptive sediment management, and effective land and water management policies throughout the MRB and other global basins.

Data Availability Statement

Some or all data, models, or code that support the findings of this study are available from the corresponding author upon reasonable request.

Acknowledgments

This work was primarily funded by The National Science Foundation Graduate Research Fellowship Program under Grant No. DGE-1762114 to the first author. This work also benefitted from NASA Earth System and Science Fellowship Grant 80NSSC17K0379 to the second author and the NASA Water Applied Science Program (Grant NNX15AC63G) to the third author. The authors would like to thank MRC, Kel Markert of the NASA/USAID SERVIR program, and ADCP for providing in situ sediment data; Kensey Daly for assistance in retrieving land cover data; and Nishan Kumar Biswas for GIS assistance.

References

Adamson, P. T., I. D. Rutherford, M. C. Peel, and I. A. Conlan. 2009. "The hydrology of the Mekong River." In *The Mekong: Biophysical environment of an international river basin*. Edited by I. C. Campbell, 53–76. Amsterdam, Netherlands: Elsevier.

Belward, A. S., J. E. Estes, and K. D. Kline. 1999. "The IGBP-DIS global 1-km land-cover data set discover: A project overview." *Photogramm. Eng. Remote Sens.* 65 (9): 1013–1020.

Brandt, S. A. 2000. "Classification of geomorphological effects downstream of dams." *Catena* 40 (4): 375–401. https://doi.org/10.1016/S0341-8162(00)00093-X.

Chander, G., L. Markham, and D. L. Halder. 2009. "Summary of current radiometric calibration coefficients for Landsat MSS, TM, ETM+, and EO-1 ALI sensors." *Remote Sens. Environ.* 113 (5): 893–903. https://doi.org/10.1016/j.rse.2009.01.007.

Cleveland, W. S. 1979. "Robust locally weighted regression and smoothing scatterplots." *J. Am. Stat. Assoc.* 74 (368): 829–836. https://doi.org/10.1080/01621459.1979.10481038.

Dang, T. D., T. A. Cochrane, and M. E. Arias. 2018. "Quantifying suspended sediment dynamics in mega deltas using remote sensing data: A case study of the Mekong floodplains." *Int. J. Appl. Earth Obs. Geoinf.* 68 (Jun): 105–115. https://doi.org/10.1016/j.jag.2018.02.008.

Federal Interagency Sedimentation Project. 1941. *Laboratory investigation of suspended-sediment samplers*, 99. Interagency Rep. No. 5. Iowa City, IA: Iowa Univ. Hydraulics Laboratory.

Friedl, M., and D. Sulla-Menashe. 2015. *MCD12Q1 MODIS/Terra+ aqua land cover type yearly L3 global 500m SIN grid V006*. NASA EOSDIS Land Processes DAAC.

Gholizadeh, M. H., A. M. Melesse, and L. Reddi. 2016. "A comprehensive review on water quality parameters estimation using remote sensing techniques." *Sensors* 16 (8): 1298. https://doi.org/10.3390/s16081298.

Gorelick, N., M. Hancher, M. Dixon, S. Ilyushchenko, D. Thau, and R. Moore. 2017. "Google Earth engine: Planetary-scale geospatial analysis for everyone." *Remote Sens. Environ.* 202 (Dec): 18–27. https://doi.org/10.1016/j.rse.2017.06.031.

ICEM (International Centre for Environmental Management). 2010. "Hydrology and sediment baseline assessment working paper." In *Baseline assessment report, strategic environmental assessment of hydropower on the Mekong mainstream for the MRC*, 85. Hanoi, Vietnam: ICEM.

Jones, J. W. 2015. "Efficient wetland surface water detection and monitoring via Landsat: Comparison with in situ data from the Everglades depth estimation network." *Remote Sens.* 7 (9): 12503–12538. https://doi.org/10.3390/rs70912503.

Koehnken, L. 2014. *Discharge sediment monitoring project (DSMP) 2009–2013 summary & analysis of results*. Final Report. Vientiane, Laos: Mekong River Commission Secretariat.

Kondolf, G. M., C. Alford, and Z. Rubin. 2011. *Cumulative effects of tributary dams on the sediment loads and channel form in the lower Mekong River: Progress report through 30 September 2011*. Berkeley, CA: Dept. of Landscape Architecture and Environmental Planning, Univ. of California.

Kondolf, G. M., Z. K. Rubin, and J. T. Minear. 2014. "Dams on the Mekong: Cumulative sediment starvation." *Water Resour. Res.* 50 (6): 5158–5169. https://doi.org/10.1002/2013WR014651.

Kondolf, G. M., et al. 2018. "Changing sediment budget of the Mekong: Cumulative threats and management strategies for a large river basin." *Sci. Total Environ.* 625 (Jun): 114–134. https://doi.org/10.1016/j.scitotenv.2017.11.361.

Kong, D., C. Miao, J. Wu, A. G. Borthwick, Q. Duan, and X. Zhang. 2017. "Environmental impact assessments of the Xiaolangdi Reservoir on the most hyperconcentrated Laden River, Yellow River, China." *Environ. Sci. Pollut. Res.* 24 (5): 4337–4351. https://doi.org/10.1007/s11356-016-7975-4.

Kummu, M., X. X. Lu, J. J. Wang, and O. Varis. 2010. "Basin-wide sediment trapping efficiency of emerging reservoirs along the Mekong." *Geomorphology* 119 (3–4): 181–197. https://doi.org/10.1016/j.geomorph.2010.03.018.

Kummu, M., and O. Varis. 2007. "Sediment related impacts due to upstream reservoir trapping, the Lower Mekong River." *Geomorphology* 85 (3–4): 275–293. https://doi.org/10.1016/j.geomorph.2006.03.024.

Loveland, T. R., and A. S. Belward. 1997. "The IGBP-DIS global 1km land cover data set, DISCover: First results." *Int. J. Remote Sens.* 18 (15): 3289–3295. https://doi.org/10.1080/014311697217099.

Lu, X. X., C. Oeurng, T. P. Q. Le, and D. T. Thuy. 2015. "Sediment budget as affected by construction of a sequence of dams in the lower Red River, Viet Nam." *Geomorphology* 248 (Nov): 125–133. https://doi.org/10.1016/j.geomorph.2015.06.044.

Mård, J., G. Di Baldassarre, and M. Mazzoleni. 2018. "Nighttime light data reveal how flood protection shapes human proximity to rivers." *Sci. Adv.* 4 (8): 1–8. https://doi.org/10.1126/sciadv.aar5779.

Markert, K. N., et al. 2018. "Historical and operational monitoring of surface sediments in the Lower Mekong Basin using Landsat and Google Earth Engine cloud computing." *Remote Sens.* 10 (6): 1–19. https://doi.org/10.3390/rs10060909.

MRC (Mekong River Commission). 2005. *Overview of the hydrology of the Mekong Basin*. Vientiane, Laos: MRC.

MRC (Mekong River Commission). 2011. *Hydrological database*. Vientiane, Laos: MRC.

MRC (Mekong River Commission). 2013. *Improved environmental & socio-economic baseline information for hydropower planning (ISH11)*. Vientiane, Laos: MRC.

MRC (Mekong River Commission). 2017. "Mekong sediment from the Mekong River commission study." http://www.mrcmekong.org/assets/Publications/Mekong-sediment-from-the-MRC-Council-Study [25] -Technical-notedocx.pdf.

NOAA–Earth Observation Group. 2016. "Version 4 DMSP-OLS nighttime lights time series." https://ngdc.noaa.gov/eog/dmsp/downloadV4 [26] composites.html.

Open Development Mekong. 2015. "Hydro basins level 6: Mekong." Accessed November 16, 2018. https://data.opendevelopmentmekong.net/dataset/hydro-basins-level-6-greater-mekong-subregion-laos-myanmar-thailand-vietnam-cambodia.

Pavelsky, T. M., and L. C. Smith. 2009. "Remote sensing of suspended sediment concentration, flow velocity, and lake recharge in the Peace-Athabasca Delta, Canada." *Water Resour. Res.* 45 (11): 1–16. https://doi.org/10.1029/2008WR007424.

Piman, T., T. A. Cochrane, and M. E. Arias. 2016. "Effect of proposed large dams on water flows and hydropower production in the Sekong, Sesan and Srepok Rivers of the Mekong Basin." *River Res. Appl.* 32 (10): 2095–2108. https://doi.org/10.1002/rra.3045.

Piman, T., and M. Shrestha. 2017. *Case study on sediment in the Mekong* [27] *River Basin: Current state and future trends*.

QGIS Development Team. 2018. "QGIS geographic information system: Version 3.4.1. Open source geospatial foundation project." http://qgis [28] .osgeo.org.

Ritchie, J. C., C. M. Cooper, and J. Yongqing. 1987. "Using Landsat multispectral scanner data to estimate suspended sediments in Moon Lake, Mississippi." *Remote Sens. Environ.* 23 (1): 65–81. https://doi.org/10.1016/0034-4257(87)90071-X.

Sarkkula, J., J. Koponen, H. Lauri, and M. Virtanen. 2010. *MRC/Information and knowledge management program detailed modelling support (DMS) project: Origin, fate and impacts of the Mekong sediments*, 53. Vientiane, Laos: Mekong River Commission.

Schmitt, R. J. P., S. Bizzi, A. F. Castelletti, and G. M. Kondolf. 2018. "Stochastic modeling of sediment connectivity for reconstructing sand fluxes and origins in the unmonitored Se Kong, Se San, and Sre Pok tributaries of the Mekong River." *J. Geophys. Res. Earth Surf.* 123 (1): 2–25. https://doi.org/10.1002/2016JF004105.

Suif, Z., A. Fleifle, C. Yoshimura, and O. Saavedra. 2016. "Spatio-temporal patterns of soil erosion and suspended sediment dynamics in the Mekong River Basin." *Sci. Total Environ.* 568 (Oct): 933–945. https://doi.org/10.1016/j.scitotenv.2015.12.134.

Volpe, V., S. Silvestri, and M. Marani. 2011. "Remote sensing retrieval of suspended sediment concentration in shallow waters." *Remote Sens. Environ.* 115 (1): 44–54. https://doi.org/10.1016/j.rse.2010.07.013.

Wackerman, C., A. Hayden, and J. Jonik. 2017. "Deriving spatial and temporal context for point measurements of suspended-sediment concentration using remote-sensing imagery in the Mekong Delta." *Cont. Shelf Res.* 147 (Sep): 231–245. https://doi.org/10.1016/j.csr.2017.08.007.

Walling, D. E. 2008. "The changing sediment load of the Mekong River." *Ambio* 37 (3): 150–157. https://doi.org/10.1579/0044-7447(2008)37[150:TCSLOT]2.0.CO;2.

Wang, J. J., and X. X. Lu. 2010. "Estimation of suspended sediment concentrations using Terra MODIS: An example from the Lower Yangtze River, China." *Sci. Total Environ.* 408 (5): 1131–1138. https://doi.org/10.1016/j.scitotenv.2009.11.057. [29]

Wei, X., S. Sauvage, T. P. Quynh Le, S. Ouillon, D. Orange, V. D. Vinh, and J. M. Sanchez-Perez. 2019. "A modeling approach to diagnose the impacts of global changes on discharge and suspended sediment concentration within the Red River Basin." *Water* 11 (5): 958. https://doi.org/10.3390/w11050958.

Wild, T., and D. P. Loucks. 2014. "Managing flow, sediment, and hydropower regimes in the Sre Pok, Se San, and Se Kong Rivers of the Mekong Basin." *Water Resour. Res.* 50 (6): 5141–5157. https://doi.org/10.1002/2014WR015457.

WLE. 2017. *Dataset on the dams of the Irrawaddy, Mekong, Red and Salween River basins*. Vientiane, Laos: CGIAR Research Program on Water, Land and Ecosystems—Greater Mekong. [30]

World Resources Institute. 2011. "Country boundaries of Southeast Asia." Accessed November 16, 2018. https://databasin.org/datasets/59c48c37d74e4a2db4dbc6997c8eba3b.

Xu, J., and Y. Yan. 2010. "Effect of reservoir construction on suspended sediment load in a large river system: Thresholds and complex response." *Earth Surf. Process. Landf.* 35 (14): 1666–1673. https://doi.org/10.1002/esp.2006.

Xu, T., T. Ma, C. Zhou, and Y. Zhou. 2014. "Characterizing spatio-temporal dynamics of urbanization in China using time series of DMSP/OLS night light data." *Remote Sens.* 6 (8): 7708–7731. https://doi.org/10.3390/rs6087708.

Yepez, S., A. Laraque, J. M. Martinez, J. De Sa, J. M. Carrera, B. Castellanos, M. Gallay, and J. L. Lopez. 2018. "Retrieval of suspended sediment concentrations using Landsat-8 OLI satellite images in the Orinoco River (Venezuela)." *Comptes Rendus Geosci.* 350 (1–2): 20–30. https://doi.org/10.1016/j.crte.2017.08.004.

Zhang, M., Q. Dong, T. Cui, C. Xue, and S. Zhang. 2014. "Suspended sediment monitoring and assessment for Yellow River estuary from Landsat TM and ETM+ imagery." *Remote Sens. Environ.* 146 (Apr): 136–147. https://doi.org/10.1016/j.rse.2013.09.033.